Title
Insights into Particle Cycling from Thorium and Particle Data

Authors
Lam, Phoebe J
Marchal, Olivier

Insights into Particle Cycling from Thorium and Particle Data

Phoebe J. Lam[1,3] and Olivier Marchal[2]

[1]Department of Marine Chemistry and Geochemistry and [2]Department of Geology and Geophysics, Woods Hole Oceanographic Institution, Woods Hole, Massachusetts 02543; email: pjlam@whoi.edu, omarchal@whoi.edu

[3]Department of Ocean Sciences, University of California, Santa Cruz, Santa Cruz, California 95064

Abstract Marine particles are a main vector by which the biological carbon pump in the ocean transfers carbon from the atmosphere to the deep ocean. Marine particles exist in a continuous spectrum of sizes, but they can be functionally grouped into a small, suspended class (which constitutes most of the total particle mass) and a large, sinking class (which contributes most of the particle flux). These two classes are connected by aggregation and disaggregation processes. The interplay of processes that create, aggregate, and destroy marine particles determines the strength and transfer efficiency of the biological pump. Measurements of radiocarbon, barium, and organic biomarkers on suspended and sinking particles have provided qualitative insights into particle dynamics, and measurements of thorium isotopes have provided quantitative estimates of rates. Here, we review what has been learned so far about particle dynamics in the ocean from chemical

measurements on suspended and sinking particles. We then discuss future directions for this approach.

1. INTRODUCTION

The biological carbon pump in the ocean plays an important role in regulating atmospheric CO_2 levels by drawing down CO_2 during photosynthesis and transferring that carbon via sinking particles to the deep ocean (Kwon et al. 2009, Volk & Hoffert 1985). Some of the most pressing questions in marine biogeochemistry concern the factors controlling the variability of export flux and its attenuation through the mesopelagic zone, which is between approximately 100 and 1,000 m.

In the context of the biological carbon pump, particle dynamics in the ocean refers to the production, aggregation, sinking, disaggregation, and remineralization of organic carbon particles (**Figure 1**). Here, we use the term aggregation to mean both abiotic (e.g., from physical coagulation) and biologically mediated (e.g., from zooplankton fecal pellet production) processes that lead to the packaging of small particles into large particles. Likewise, we use the term disaggregation to mean both abiotic (e.g., from shear stress) and biologically mediated (e.g., from zooplankton fragmentation) processes that lead to the breakdown of large particles into small particles. The interplay of these processes is thought to determine the strength [magnitude of particulate organic carbon (POC) flux] and the transfer efficiency (remineralization length scale of POC flux profile) of the biological pump. Broadly, the attenuation of vertical POC flux with depth reflects the balance between (*a*) processes that promote the formation of sinking particles (such as aggregation), which promote efficient transit through the water column and thus lessen the attenuation, and (*b*) processes that promote the destruction of sinking particles (such as disaggregation and remineralization), which accentuate it.

<COMP: PLEASE INSERT FIGURE 1 HERE>

Figure 1 Schematic depiction of the biological carbon pump, emphasizing the important particle dynamics processes: aggregation (*red arrows*), sinking (*black arrows*), disaggregation (*dark blue arrows*), and remineralization (*light blue arrows*).

Particles in the small, suspended size fraction (*brown*) comprise phytoplankton, authigenic particles, and lithogenic particles. They do not sink or sink very slowly. Particles in the large, sinking size fraction (*green*) comprise fecal material and aggregates of smaller particles and do sink. Aggregation can be abiotic (physical) or mediated by zooplankton packaging through fecal pellet production (biological). Disaggregation can result, for example, from shear stress or can be biologically mediated. In this conceptual model, particles in the suspended size fraction (*brown*) decrease with depth because of remineralization.

Although a prime motivation for studying particle dynamics is to understand the cycling of carbon, marine particles comprise much more than just POC. They are a heterogeneous mix of biogenic components and authigenic minerals that are produced internally in the water column and components such as lithogenic material that are derived externally to the water column (see Fowler & Knauer 1986, Jeandel et al. 2014). In most open-ocean environments, biogenic material—which includes particulate organic matter and biogenic minerals such as calcium carbonate ($CaCO_3$) and biogenic silica (opal)—dominates particle mass (e.g., Bishop et al. 1977, François et al. 2002). In environments close to ocean margins or influenced by atmospheric dust deposition, lithogenic material can also be important (Lam et al. 2014). Authigenic minerals such as barite ($BaSO_4$) and iron and manganese oxyhydroxides are typically minor components of particle mass, except in special environments such as hydrothermal vent plumes, where oxyhydroxides can be a significant component (Lam et al. 2014). Many other trace elements and isotopes have a particulate component that is important to their cycling, but these elements and isotopes are not important components of particulate mass.

Because organic matter is such an important component of particle mass, the biologically mediated processes governing its production, aggregation, and destruction (**Figure 1**) also control the cycling of abiotic and trace particle components. The dominance of the processes cycling POC in the ocean allows the same framework of particle interactions to be used to understand the distributions of minor particulate components. Conversely, it also allows minor particulate constituents to be used as tracers of particle dynamics.

In this review, we describe the conceptual framework for particle dynamics that arose from studies of the geochemistry of suspended and sinking particles. Much of this work was pioneered in the 1980s and 1990s using thorium, a particle-reactive

3

radioisotope, as a tracer of particle dynamics. The use of Th isotope data to infer rate constants has received little attention in the past 15 years, likely because of large errors in these constants. However, the international GEOTRACES program (Anderson et al. 2014) is generating an unprecedented set of thorium isotope and particle concentration measurements on different size fractions, which could significantly reduce the error in estimates of rate constants (Marchal & Lam 2012). Moreover, a significant intercalibration effort has already been undertaken to ensure the comparability of measurements from different laboratories (Cutter 2013). It is thus timely to revisit previous studies on particle cycling in the ocean, as the concurrent measurement of many particulate components as part of the GEOTRACES program could potentially add even more observational constraints. This article therefore reviews what has been learned about particle dynamics from chemical measurements on particulate samples, discusses why a simple two-particle-class model still provides a useful and unifying conceptual framework for understanding the distributions of many seemingly unrelated particulate elements, and speculates on the way forward.

2. APPROACHES TO STUDYING PARTICLE DYNAMICS

Marine particles exist in a continuous spectrum of sizes. The number of particles per water volume as a function of particle diameter is typically described by a power law for particles greater than 1 µm (Brun-Cottan 1986). The smallest particles are the most numerous, and the exponent of the power law describes the particle size distribution (Burd & Jackson 2009, McCave 1984, Stemmann & Boss 2012). Particles are acted upon by physical and biological processes that lead to transformations between sizes through particle production, aggregation, disaggregation, and remineralization. These transformations fall under the umbrella of particle dynamics.

Three main approaches are currently used to study particle dynamics: (*a*) applying coagulation theory to understand the physical aggregation of marine particles, (*b*) directly measuring the biologically mediated rates of particle transformations, and (*c*) inferring rates based on the quantitative combination of simple models with

4

measurements of the chemical composition (especially particle-reactive radioisotopes) of suspended and sinking particles. Coagulation theory provides a richly developed framework for understanding the physical aggregation of particles. McCave (1984) was one of the first to use elements of coagulation theory to describe the physical aggregation of marine particles. Coagulation theory has been more recently used to predict maximum particle concentrations in phytoplankton bloom situations [see review by Burd & Jackson (2009)]. New optical and imaging techniques have made it easier to measure particle size spectra in the ocean (Stemmann & Boss 2012), providing a measurable target for testing aspects of coagulation theory (Burd & Jackson 2009, McCave 1984). A disadvantage of this theory, however, is that it does not specifically account for biologically mediated particle transformation processes, such as zooplankton production of fecal pellets, or for disaggregation.

The second approach to studying particle dynamics is to measure the rates of growth, assimilation, and respiration of the key biological actors—phytoplankton, zooplankton, and bacteria—that mediate some of the key particle transformations (Giering et al. 2014, Steinberg et al. 2008). Although these organisms are key agents of particle dynamics, this approach ignores physical aggregation and disaggregation processes, and even biologically mediated aggregation and disaggregation processes are not measured directly.

The third approach is to regard marine particles as being composed of a finite, very small number of classes of different sizes. For example, particles can be grouped into two classes: a small, suspended class and a large, sinking class (**Figure 2**). Chemical measurements on the two classes can then be used to infer the rates of aggregation and disaggregation that connect them. Although classifying marine particles into two classes is a clear simplification of reality (see Burd 2013), it complies with the operational definition of suspended and sinking particles in modern sampling techniques (Bishop et al. 2012, McDonnell et al. 2014) so that net rates of interest can be directly constrained. Furthermore, this approach captures and distinguishes the key characteristics of particles in the ocean: Most of the particle mass in the ocean is made up of small, suspended particles with relatively long

residence times (months to years), whereas most of the vertical mass flux is carried out by relatively rare, large, sinking particles with short residence times (days) (Bacon et al. 1985, Bishop et al. 1977, Clegg & Whitfield 1990, McCave 1975, Nozaki et al. 1987). However, the physical or geochemical interpretation of the inferred rate constants can be ambiguous, and their very value can be biased owing to the simplistic nature of the two-particle class model. Note that whereas some chemical measurements (e.g., Δ^{14}C, barite, and organic biomarkers) can provide a qualitative understanding of particle dynamics, other measurements (e.g., thorium isotopes and lithogenic particles) can provide a quantitative estimate of rates (see Section 3).

<COMP: PLEASE INSERT FIGURE 2 HERE>

Figure 2 Particle dynamics framework showing the interactions between the dissolved fraction (Diss.), small particles (P_S), and large particles (P_L) as applied to four components, together with the typical concentration profiles of these components: (*a*) thorium (^{230}Th, a particle-reactive radionuclide), (*b*) particulate organic carbon (POC, a biogenic compound), (*c*) barite (pBa, an authigenic mineral), and (*d*) particulate titanium (pTi, a lithogenic element). All four components experience aggregation (β_2), disaggregation (β_{-2}), and sinking (*w*). Sources (*colored boxes*) and interactions with the dissolved phase vary for each component. The sources are radioactive production (λ_U) for ^{230}Th, primary production (PP) for POC, authigenic precipitation (AP) for pBa, and dust deposition (DD) for pTi. The interactions with the dissolved phase include adsorption (k_1), desorption (k_{-1}), remineralization (β_{-1}), and dissolution (δ). Titanium is very insoluble in seawater, so dissolved titanium (dTi) can be disregarded in the interpretation of particulate profiles. The horizontal blue line separates the euphotic zone from the mesopelagic zone. The example concentration profiles for each element show the small (*dashed line*) and large (*solid line*) size fractions. The p^{230}Th profiles are idealized; the POC, pBa, and pTi profiles are taken from the US GEOTRACES North Atlantic Zonal Transect (D.C. Ohnemus & P.J. Lam, unpublished data). Additional abbreviations: d, dissolved; DIC, dissolved inorganic carbon; dpm, disintegrations per minute.

In summary, the benefit of the first two approaches (coagulation theory and biological rate measurements) is that they are mechanistically based strategies that allow prediction and testing of particle dynamics behavior; however, neither one alone captures all the relevant processes. The net effect of particle aggregation and disaggregation is ultimately the result of a combination of various physical (e.g., coagulation) and biological (e.g., fecal pellet production) mechanisms and is likely

to vary spatially and temporally. The advantage to the third, geochemical approach is that it does not require knowledge about which specific physical or biological processes are responsible for the particle transformations. When using certain geochemical tracers like thorium isotopes, this appears to be the only approach that can specifically provide quantitative estimates of net rates of aggregation and disaggregation, both of which may be impossible to measure directly. However, the geochemical approach has the disadvantage that it does not provide insight into the detailed processes and mechanisms that contribute to the inferred rate constants. Thus, the three approaches described above should be viewed as complementary. In the remainder of this article, we review what has been learned about particle dynamics from this third approach—that is, inferring particle dynamics processes from the chemical composition of suspended and sinking particles.

3. THE TWO-PARTICLE-CLASS MODEL

Particle collection for chemical analysis is typically accomplished through filtration or by sediment traps (Bishop et al. 2012, Buesseler et al. 2007, Fowler & Knauer 1986, McDonnell et al. 2014). Particles collected through filtration typically represent suspended particles, and particles collected by sediment traps represent sinking particles. Large-volume filtration using in situ pumps allows size fractionation so that sinking particles can be approximated by the large size fraction, most commonly defined as particles larger than 53 μm or 70 μm (Abramson et al. 2010, Bishop et al. 1977, Buesseler et al. 1995, Cochran et al. 2000, Lam & Bishop 2007). Chemical measurements on suspended and sinking particles can then provide information about the exchanges between the two classes. The sinking speed of a particle derived from a balance between the buoyancy force and the viscous drag force (Stokes' law) is proportional to the square of its diameter and to its excess density over seawater (e.g., Komar et al. 1981). Because of the sensitivity of sinking speed to particle size, size fractionation is an operationally defined method to separate suspended and sinking particles. However, laboratory experiments and field-based estimates have shown that particle sinking rate is not always a monotonic function of particle size (Engel et al. 2009, Iversen & Ploug 2010,

McDonnell & Buesseler 2010), suggesting that particle density and/or shape can also exert an important role. Although size fractionation is an imperfect operational separation of suspended and sinking particles, there is evidence that large particles collected from in situ filtration can be chemically more similar to sinking particles collected from sediment traps than to the small size fraction (Abramson et al. 2010).

Bacon et al. (1985) observed large temporal variations in ^{230}Th flux in sediment trap samples near Bermuda even when the ^{230}Th concentration in the particles caught in the trap was not changing. The authors concluded that this observation was most consistent with a conceptual model in which (*a*) a suspended fraction of particles that make up the bulk of total particle mass is responsible for the scavenging of ^{230}Th from the water column, (*b*) a small fraction of total particle mass is responsible for the majority of the flux, and (*c*) these two fractions are connected by aggregation and disaggregation processes. Indeed, the persistence of particles in both suspended and sinking size fractions throughout the water column implies that aggregation and disaggregation processes occur throughout the water column.

Bomb radiocarbon has been used as a tracer of surface-derived particles. The radiocarbon activity (as expressed by Δ^{14}C, which corrects for isotopic fractionation effects) of sinking POC from deep (>4,000 m) sediment traps in the central North Pacific was virtually the same as that of surface dissolved inorganic carbon (DIC) and POC values, confirming the presence of a rapidly sinking, surface-derived pool of particles (Druffel & Williams 1990). The Δ^{14}C of suspended POC below the euphotic zone, by contrast, was lower than that of sinking POC but higher than that of either the corresponding ambient DIC or dissolved organic carbon (DOC), suggesting that it was a longer-lived pool that derived from the disaggregation of quickly sinking particles but had adsorbed radiocarbon-depleted DOC (Druffel & Williams 1990). These data support the notion that particles can be grouped into a rapidly sinking, surface-derived pool and a longer-lived suspended pool that has more time to interact with the dissolved phase.

Further evidence that large, sinking particles are functionally distinct from small, suspended particles comes from studies of the organic chemical compositions of

these particles. Lipid biomarkers show that suspended and sinking particles from the North Pacific are geochemically distinct: Suspended particles contain lipids derived from both phytoplankton and zooplankton sources, whereas sinking particles contain primarily lipids derived from zooplankton sources (Wakeham & Canuel 1988).

Because multiple geochemical tracers support the idea of two functional particle classes, we focus here on an idealized two-size-class particle model in which small, suspended particles do not sink but rather interact with the dissolved phase through scavenging, dissolution, and/or remineralization (depending on the element) and are aggregated physically by impaction and/or biologically by fecal pellet production into large, sinking particles (Burd & Jackson 2009, Clegg et al. 1991). Large particles sink and disaggregate because of processes such as shear stress, sloppy feeding, and/or microbial breakdown of fecal membranes into small, suspended particles. We further assume that the aggregation and disaggregation processes that connect the two particle size classes occur throughout the water column (**Figure 1**), although studies have shown that these can vary geographically and seasonally (Abramson et al. 2010, Wakeham & Canuel 1988). The reactions between the dissolved, suspended, and sinking particulate pools are typically represented as first-order processes (Clegg & Whitfield 1991, Murnane 1994, Nozaki et al. 1987).

This basic framework (**Figure 1**) can be applied to multiple types of particulate elements that, because of their different vertical distributions, at first glance appear to be controlled by different processes. Simply by varying the source for the element under consideration and the interactions between the dissolved and suspended particle phases, one can use this framework to describe the distribution of many particulate elements. **Figure 2** demonstrates the versatility of this model as applied to four particulate components that have very different sources: ^{230}Th (a particle-reactive radionuclide), POC (a biogenic compound), barite (an authigenic mineral), and titanium (a lithogenic element). Despite their dramatically different vertical distributions, the behaviors of all four components are consistent with the general particle dynamics framework with sinking of large particles and particle aggregation and disaggregation throughout the water column. Below, the cycling of each of these components is discussed in turn.

3.1. ^{230}Th: Uniform Production Throughout the Water Column

The development of this overall particle dynamics framework arose from studies of the particle-reactive thorium isotopes. The vertical profiles of dissolved and particulate ^{230}Th show generally increasing values with depth (Bacon & Anderson 1982, Nozaki et al. 1981) (**Figure 2a**). ^{230}Th is produced by the radioactive decay of ^{234}U. Because uranium is approximately conservative in the ocean, ^{230}Th has an approximately constant production throughout the water column. This contrasts with most other tracers, which have sources at particular depths (often the surface), and is one reason that the depth profile of ^{230}Th is so distinctive.

The increasing concentration of ^{230}Th with depth can be explained by a constant source coupled with reversible exchange (adsorption and desorption) and vertical removal by sinking particles (Bacon & Anderson 1982, Nozaki et al. 1981). This original model did not separate suspended from sinking particles. The explicit addition of a quickly sinking particle size class as separate from the suspended class further allowed the estimation of particle aggregation and disaggregation rate constants (Nozaki et al. 1987) (**Figure 2a**). Section 4.1 further discusses thorium-based estimates of particle dynamics.

3.2. Particulate Organic Carbon: A Biogenic Source in the Euphotic Zone

The model for a biogenic phase such as POC (**Figure 2b**) is the stripped-down view of the biological pump presented in **Figure 1**: Small, suspended particles (i.e., phytoplankton) are produced by photosynthesis [primary production (PP)] from the DIC pool in the euphotic zone. These small particles are subject to remineralization (β_{-1}), or are aggregated (β_2) into large particles via coagulation or zooplankton-mediated packaging, and the large particles sink (w) out of the euphotic zone. Large particles continue sinking throughout the water column, where they disaggregate (β_{-2}) into small, suspended particles, which are in turn subject to remineralization or reaggregation. This dynamics sets up concentration profiles for both small- and large-particle size fractions that are maximal in the euphotic zone, where particles are produced, and that rapidly decrease with depth as particles are disaggregated and remineralized. The model for POC (**Figure 2b**) was explicitly devised in the same form as the thorium model (**Figure 2a**) so that both models can be jointly considered

for the interpretation of field measurements (cf. Clegg & Whitfield 1990, Murnane et al. 1990). Coupling the two models added observational constraints and allowed the scavenging processes [i.e., desorption (k_{-1})] to be separated from the particle cycling processes [i.e., remineralization (β_{-1})].

3.3. Barite: An Authigenic Source in Large Aggregates

Sedimentary barite is used as a proxy for past biological productivity (Paytan & Griffith 2007), so its behavior in the water column is of interest (Dymond et al. 1992, François et al. 1995). The conceptual framework in which large particles disaggregate to small, suspended particles has been critical for understanding the systematics of particulate barium profiles.

Particulate barium in the water column is dominated by the authigenic mineral barite ($BaSO_4$) (Dehairs et al. 1980). Because barite is undersaturated in the water column, it is thought to form in microenvironments of large, siliceous aggregates, where barite saturation can be reached from elevated sulfate levels created by decomposing organic matter (Bishop 1988, Dehairs et al. 1980). Microscopic examination of large aggregates has shown that the barite particles formed in aggregates are micron sized. The depth profiles of particulate barium often show a surface maximum in the large-particle size fraction that decreases with depth, and a surface minimum in the suspended size fraction that increases quickly with depth below the euphotic zone (Bishop 1988) (**Figure 2c**). Because the concentration of large aggregates is greatest in the surface waters (see the large-POC concentration profile shown in **Figure 2b**), the abundance of aggregate-hosted microenvironments explains the surface maximum in barium in the large-particle size fraction. As these large particles sink and disaggregate, the micron-sized barite crystals are released into the suspended size fraction, where they accumulate at the depth of the most intense disaggregation. The suspended barium profiles typically show a maximum in the upper mesopelagic zone, where disaggregation is greatest, and a decrease with depth as individual barite crystals dissolve in the undersaturated water column (Bishop 1988, Bishop & Wood 2008, Bishop et al. 2012, Dehairs et al. 1980, Jeandel et al. 2000). Note that the suspended barium maximum does not correspond

to the suspended particle maximum, which, like POC, is typically observed in surface waters (**Figure 2***b,c*).

A correlation between the inventory of suspended barium in the mesopelagic zone with apparent oxygen utilization has led to its use as a proxy for bacterial remineralization rate (Dehairs et al. 2008). In the conceptual model described above, the remineralization estimated by this proxy must be closely linked to large-particle disaggregation (see Clegg et al. 1991). The maintenance of large-particle barium concentrations with depth seems to imply continual aggregation to balance the disaggregation. Indeed, observations of increasing barium flux with depth in the mesopelagic zone at the Ocean Flux Program site near Bermuda could be explained either by deep aggregation or by in situ production (Huang & Conte 2009).

3.4. Titanium: An Atmospheric Dust Source

The depth profiles of dust-derived lithogenic elements such as titanium show a surface maximum in both the suspended and sinking size fractions (likely caused by dust deposition), a rapid decrease in the suspended size fraction just below the mixed layer, and a rapid increase in the upper mesopelagic zone (Ohnemus & Lam 2014) (**Figure 2***d*). Assuming no lateral inputs of lithogenic material, the only source of particulate titanium to the ocean is the atmospheric deposition of mineral dust. Furthermore, assuming that the deposition is occurring far enough away from the dust-source region, so that only fine (micron to tens of microns) particles of dust can be transported to the sampling location, the deposited particulate titanium should be only in the suspended particulate size fraction (Ratmeyer et al. 1999); any titanium in the large size fraction must therefore be a result of aggregation.

Titanium has no known biological function and is among the least soluble of the lithogenic elements—3% of aerosol titanium is soluble in distilled water, compared with 15% for aluminum and iron (Buck et al. 2010). The relatively low susceptibility of titanium to scavenging (Dammshäuser et al. 2013) further suggests that, in areas of dust deposition, particulate titanium is dominated by a refractory phase that can be thought of as an inert tracer of particle processes, with a single source to the surface ocean and its only removal coming from aggregation into large sinking particles (Ohnemus & Lam 2014). The observed profile of size-fractionated

particulate titanium can then be simulated using a model with depth-dependent aggregation and disaggregation rate constants (Ohnemus & Lam 2014). As with barite, particulate titanium is transported below the euphotic zone by large sinking particles, which then disaggregate and release the fine lithogenic particles back into the suspended phase.

4. INFERENCES ABOUT PARTICLE DYNAMICS FROM THORIUM ISOTOPE AND PARTICLE DATA

In Section 3, examples of particulate profiles were united by a common framework that considers aggregation, disaggregation, and sinking processes and were distinguished by their different sources and interactions with the dissolved phase. In this section, we discuss the specific insights provided by different geochemical tracers.

4.1. Rate Constants and Turnover Times

The most quantitative understanding of particle dynamics comes from the application of thorium isotopes. There are three reasons that thorium isotopes are so useful for studying particle dynamics: (*a*) Their source is relatively well known [they are produced from the radioactive decay of uranium ($^{238}U \rightarrow {}^{234}Th$, $^{234}U \rightarrow {}^{230}Th$) or radium ($^{228}Ra \rightarrow {}^{228}Th$), whose activities in seawater can be measured or estimated]; (*b*) they are particle-reactive but not thought to be biologically active, so their removal comes from their radioactive decay (which is known) and from scavenging onto settling particles; and (*c*) thorium has several isotopes measurable in seawater, which have very different half-lives ($t_{1/2}$ = 24.1 days, 1.91 years, and 7.54×10^4 years for ^{234}Th, ^{228}Th, and ^{230}Th, respectively) but are all expected to behave the same way chemically, providing multiple constraints on thorium and particle cycling (Anderson 2003).

From the simple conceptual model presented in **Figure 2*a***, the following equations can be written to describe, for each thorium isotope, the time rate of change for the activities of dissolved (Th_d), small particulate (Th_S), and large particulate (Th_L) phases:

$$\frac{\partial Th_d}{\partial t} = \lambda P - (k_1 + \lambda) \cdot Th_d + (k_{-1} + \beta_{-1}) \cdot Th_S, \quad (1)$$

$$\frac{\partial Th_S}{\partial t} = k_1 \cdot Th_d - (\lambda + k_{-1} + \beta_{-1} + \beta_2) \cdot Th_S + \beta_{-2} \cdot Th_L, \quad (2)$$

$$\frac{\partial Th_L}{\partial t} = \beta_2 \cdot Th_S - (\lambda + \beta_{-2}) \cdot Th_L - \frac{\partial}{\partial z}(Th_L \cdot w). \quad (3)$$

In general, the following quantities in Equations 1–3 are unknown: the adsorption (k_1), desorption (k_{-1}), remineralization (β_{-1}), aggregation (β_2), and disaggregation (β_{-2}) rate constants and the particle sinking speed (w). For the rest of this article, we refer to the five rate constants and sinking speed as model parameters. The decay constant, λ, is considered to be known. Finally, the activity of the parent, P, and the activities of the daughter thorium isotopes in the three phases, Th_d, Th_S, and Th_L, can be measured. With six unknowns and three equations, the system (Equations 1–3) is formally underdetermined if only one thorium isotope is measured.

The analogous equations to Equations 2–3 can be written for POC:

$$\frac{\partial POC_S}{\partial t} = PP - (\beta_{-1} + \beta_2) \cdot POC_S + \beta_{-2} \cdot POC_L, \quad (4)$$

$$\frac{\partial POC_L}{\partial t} = \beta_2 \cdot POC_S - \beta_{-2} \cdot POC_L - \frac{\partial(POC_L \cdot w)}{\partial z}. \quad (5)$$

Coupling the particle model (Equations 4–5; **Figure 2b**) to the thorium model (Equations 1–3; **Figure 2a**) adds two more equations without increasing the number of unknowns (assuming POC_S and POC_L data are available), thereby reducing the degree of formal underdeterminacy. This has the additional advantage of permitting the separation of desorption (k_{-1}) from remineralization (β_{-1}). Both of these processes turn small particulate [230]Th back into dissolved [230]Th (**Figure 2a**), but they do so by different mechanisms (Clegg & Whitfield 1991). If one assumes steady state and a particular sinking speed (e.g., Clegg et al. 1991), then the system represented by Equations 1–5 would be formally just-determined, and a unique solution yielding k_1, k_{-1}, β_{-1}, β_2, and β_{-2} may exist. Clearly, the coupling of the particle and thorium models assumes that

14

processes that affect POC (aggregation, sinking, disaggregation, and remineralization) are the same as those that affect the thorium cycle.

If one is interested only in the three parameters β_2, β_{-2}, and w (hereafter referred to as dynamical parameters), then Equation 3 can be solved simultaneously for three thorium isotopes (e.g., ^{234}Th, ^{228}Th, and ^{230}Th), which should be affected by the same processes. In practice, this approach has been used with two thorium isotopes and an assumed sinking speed based on values from the literature (Cochran et al. 1993, 2000). The assumed sinking speed of particles has been typically based on independent estimates using a number of methods, including in situ observation by divers (Alldredge & Gotschalk 1988), tracing of flux events between trap depths (Honjo & Manganini 1993), and the use of settling velocity sediment traps (Peterson et al. 2005).

If one combines measurements for all three thorium isotopes and particle concentrations, then the system is formally overdetermined, and least squares techniques can be used to find a solution. Note that the system represented by Equations 1–5 can be discretized using finite differences, so that the resulting set of difference equations can be expressed in compact form as a matrix equation;

$$\mathbf{E}\mathbf{x} + \mathbf{n} = \mathbf{y} \qquad (6)$$

Here, $\mathbf{E}$ is a matrix including the thorium isotope and particle data; $\mathbf{x}$ is a vector of unknowns (the model parameters k_1, k_{-1}, β_{-1}, β_2, β_{-2}, and w); $\mathbf{y}$ is a vector including (*a*) the production rates from the radioactive parents and (*b*) the boundary conditions (e.g., the flux of particulate thorium or of particles at the base of the euphotic zone); and $\mathbf{n}$ is a vector of errors in $\mathbf{y}$. In appearance, the Equation 6 is a linear estimation problem that could be solved for $\mathbf{x}$ using, e.g., any variant of the least squares approach (e.g., Wunsch 2006). In reality, however, the elements of the matrix $\mathbf{E}$ are not perfectly known because the data inevitably contain errors, which can be very significant in some cases. As a result, the estimation problem should be better expressed as

$$(\mathbf{E} + \Delta\mathbf{E})\mathbf{x} + \mathbf{n} = \mathbf{y}, \quad (7)$$

where $\mathbf{\Delta E}$ is another matrix that represents the errors in the thorium isotope and particle data. Errors resulting from elements of $\mathbf{E}$ not being perfectly known are referred to as errors in the regressors or errors in variables. Failure to recognize the nonlinear character of the estimation problem by treating $\mathbf{E}$ as known can lead to significant bias errors in the least squares and related solutions (see the discussion in Wunsch 2006, section 3.7, along with the references therein).

Among the techniques that can be used to solve the nonlinear estimation problem (Equation 7) is the method of total inversion created by Tarantola & Valette (1982), which was later extended to include model errors (Mercier 1986). This method can incorporate uncertainties in the measurements and in the a priori estimates of model parameters (the rate constants and particle settling speed) in order to find a solution that is consistent with all available information (Murnane 1994). Notably, this method also provides a formal estimate of the error in the solution and can be applied to over- or underdetermined systems. It has been used to estimate model parameters for thorium and particle cycling at Ocean Station Papa (Murnane 1994), at the Nares Abyssal Plain in the oligotrophic North Atlantic (Murnane et al. 1994), in the Joint Global Ocean Flux Study (JGOFS) North Atlantic Bloom Experiment (NABE) (Murnane et al. 1996), and in synthetic GEOTRACES data (Marchal & Lam 2012). The pros and cons of using the method of total inversion for inferring model parameters have been discussed by Athias et al. (2000a,b) and Marchal & Lam (2012).

To our knowledge, there are eight thorium data sets from which particle aggregation and/or disaggregation rate constants have been estimated (**Table 1**). We classify the methods for estimating rate constants as (*a*) direct, where rate constants are calculated by solving simultaneous equations analytically with no formal consideration of data errors, and (*b*) indirect, where rate constants are estimated by least squares inverse methods. A least squares method combining multiple constraints can significantly reduce the errors in model parameter estimates compared with the large propagated errors that often result from analytical techniques (compare, e.g., the results from Cochran et al. 1993 and Murnane et al. 1996).

The data sets studied have spanned various oceanic environments, including oligotrophic regimes (Murnane et al. 1994), eutrophic coastal inlets (Lavelle et al. 1991), the euphotic zone, and the deep abyss. The highest aggregation rate constants ($\beta_2 \approx 600$ per year) and thus shortest turnover time with respect to aggregation ($\tau_{agg} = \beta_2^{-1} \approx 0.6$ days) were estimated for particles at 125–250-m depth in the central equatorial Pacific upwelling region (Dunne et al. 1997). Conversely, the highest disaggregation rate constants ($\beta_2 \approx 5,000$ per year) and shortest turnover time with respect to disaggregation ($\tau_{disagg} = \beta_{-2}^{-1} \approx 0.07$ days) were estimated for particles at 10–105-m depth in the Ross Sea spring bloom (Cochran et al. 2000). The lowest aggregation ($\beta_2 \approx 0.02$ per year) and disaggregation ($\beta_{-2} \approx 16$ per year) rate constants were estimated for the eastern equatorial Pacific (Clegg et al. 1991). An even lower disaggregation rate constant ($\beta_{-2} \approx 0.8$ per year) estimated for Ocean Station Papa (Murnane et al. 1990) was later revised considerably upward by the lead author using a different least squares method (Murnane 1994).

<COMP: PLEASE INSERT TABLE 1 HERE>

Although real spatial and temporal variability most likely exists for these rate constants, the assumptions and methods used in each study are different enough that the values cannot be easily compared. For example, all of the studies that used direct methods to solve for rate constants (**Table 1**) made assumptions about one or more of the rate parameters, many of which varied from study to study. Even least squares methods resulted in very different estimates depending on the regression technique employed and on the errors assumed in the measurements and in the a priori estimates of the model parameters (Murnane 1994). For example, three methods were used to estimate rate constants from the same data set at Ocean Station Papa (Clegg et al. 1991, Murnane 1994, Murnane et al. 1990). In these three studies, aggregation rate constants from waters deeper than 1,000 m were found to be fairly similar and ranged from 0.2 to 0.8 per year, but disaggregation rate constants ranged from 0.8 to 400 per year, with uncertainties up to 10,000 per year.

Further caveats relate to the various assumptions underlying the two-particle-class model. For simplicity, early thorium-based studies assumed that all processes, including particle aggregation, obey first-order kinetics (Nozaki et al. 1987), and

subsequent studies have followed suit (Clegg & Whitfield 1990, 1991; Clegg et al. 1991; Cochran et al. 1993, 2000; Marchal & Lam 2012; Murnane et al. 1990, 1994, 1996). However, studies of physical particle aggregation using a size spectrum approach have emphasized the second-order nature of two particles colliding to cause aggregation (Burd & Jackson 2009). Burd (2013) recently compared a particle size spectrum approach that models particle aggregation using coagulation theory to three two-size-class particle models. These models assume (*a*) first-order kinetics for aggregation between small particles, as is done, to our knowledge, with all the thorium-based models; (*b*) second-order kinetics for aggregation between small particles; or (*c*) second-order kinetics for aggregation, allowing small particles to also aggregate with large particles. He noted that the first-order model predicts particle volumes that increase exponentially with time and never reach steady state, whereas all the other models do reach steady state. He additionally noted that the exponentially increasing particle volume in the steady-state model may be one reason that the thorium models predict disaggregation rate constants that are usually a factor of 10 or more higher than aggregation rate constants (**Table 1**). More sophisticated models that may include second-order rate formulations should be tested.

Despite the caveats described above, it remains instructive to examine variations in estimated particle dynamics rate constants within a particular study as a function of depth, seasonal progression, or geographic location.

4.2. Depth Variations in Disaggregation

Depth-dependent aggregation and disaggregation rate constants have been estimated for data sets from four locations: the Nares Abyssal Plain, the eastern equatorial Pacific, Ocean Station Papa (eastern subarctic Pacific), and the Ross Sea. The large variability in the estimates of aggregation and disaggregation made it difficult to determine whether there was a depth dependence in the Ross Sea (Cochran et al. 2000), so here we focus on the three other data sets.

Using [234]Th and particle concentration and flux data, Clegg et al. (1991) found that both aggregation and disaggregation rate constants at two stations in the eastern equatorial Pacific decreased quickly from the euphotic zone ($\beta_2 = 8–39$ per year, β_{-2}

18

= 664–2,809 per year) to 450 m (β_2 = 0.04–0.24 per year, β_{-2} = 60–66 per year) (**Table 2**). These aggregation rate constants imply small-particle turnover times of several weeks in the euphotic zone and years to decades in the upper mesopelagic zone, and large-particle turnover times of only hours to days. Aggregation decreased more quickly with depth than disaggregation, so that the ratio of disaggregation to aggregation increased from ~75 in the euphotic zone to ~300–1,600 at 450 m.

At Ocean Station Papa, no particle flux data were available, so Clegg et al. (1991) applied median disaggregation rate constants from the eastern equatorial Pacific study to calculate depth-dependent aggregation rate constants. With this assumption, they found that aggregation rate constants decreased more slowly with depth at Ocean Station Papa than in the eastern equatorial Pacific, leading to considerably lower disaggregation:aggregation (β_{-2}/β_2) ratios below the euphotic zone. At face value, lower β_{-2}/β_2 ratios should promote a higher abundance of large particles and thus higher vertical particle flux through the water column, but it is important to remember the assumptions that are applied and the generally large uncertainty in the estimated values. Nevertheless, for both data sets, the β_{-2}/β_2 ratio increased with depth, pointing to the increasing importance of large-particle destruction processes with depth.

<COMP: PLEASE INSERT TABLE 2 HERE>

It seems reasonable to expect that both biologically and physically mediated aggregation and disaggregation processes would be more active in the euphotic zone, which has higher particle concentrations than deeper waters. However, the opposite was found in a study of the oligotrophic Nares Abyssal Plain in the northwest Atlantic; at this location, aggregation rate constants were estimated to increase between the surface and 300 m before decreasing again to approximately 1,500 m (Murnane et al. 1994) (**Table 2**). Because there were very few particle flux data and no large-particle concentration data, the authors assumed a vertical distribution of both particle flux and large-particle concentrations in their analysis. Whereas the observed small-particle concentration dropped sharply with depth from the surface, the imposed large-particle concentration profile was roughly constant, and the flux profile increased with depth in the upper ocean. By contrast,

observations have shown that both large-particle concentrations (Lam et al. 2011) and particle flux (Boyd & Trull 2007, Buesseler & Boyd 2009) decrease quickly with depth below the euphotic zone. The depth trends in the particle dynamics rate constants in this study are thus not likely to be realistic given their assumed vertical profiles, especially in the upper mesopelagic zone. Between 300 m and 1,500 m, however, Murnane et al. (1994) estimated that the aggregation rate constant decreases and the β_{-2}/β_2 ratio increases, and both β_2 and β_{-2} then remain relatively constant to the ocean bottom. In this study, the small-particle turnover time with respect to aggregation was inferred to be on the order of only 3–5 weeks throughout the entire water column, and the large-particle turnover time was estimated to be less than 1 day.

For all three data sets, the estimated small-particle turnover times with respect to aggregation in the euphotic zone were of days to weeks, broadly consistent with a previous estimate of POC residence time in surface waters of the Southern California Bight of 3–100 days (Eppley et al. 1983). Estimates of small-particle turnover times in the mesopelagic zone varied much more widely, however, ranging from weeks to decades. Note that the assumptions and methods for estimating rate constants in the Clegg et al. (1991) and Murnane et al. (1996) studies were quite different, so it not clear whether the wide range in these estimates reflects true geographic variability or rather methodological differences.

4.3. Horizontal Variations and Temporal Trends in Productivity

Dunne et al. (1997) examined particle dynamics from [234]Th and size-fractionated POC measurements taken on a meridional transect across a productivity gradient during the JGOFS Equatorial Pacific Process Study (EqPac) Survey II cruise. The authors assumed a fixed and fast disaggregation rate constant of 1,825 per year based on a model of the North Atlantic Bloom Experiment (Clegg & Whitfield 1993). They found that aggregation rate constants in both the euphotic (0–100 m) and upper mesopelagic (125–250 m) zones generally increased with primary production and that the rate constants in the euphotic zone were generally higher than those in the mesopelagic zone (**Figure 3**). Because of the fixed disaggregation rate constants, these results imply decreasing β_{-2}/β_2 ratios with increasing

productivity. There was a stronger variation of β_{-2}/β_2 in the euphotic zone than in the mesopelagic zone as a function of primary productivity (**Figure 3**).

<COMP: PLEASE INSERT FIGURE 3 HERE>

Figure 3 Variations in (*a*) aggregation rate constants and (*b*) ratios of disaggregation to aggregation rate constants with integrated primary production in the central equatorial Pacific during the Joint Global Ocean Flux Study (JGOFS) Equatorial Pacific Process Study (EqPac) Survey II cruise for two depth ranges: the euphotic zone (0–100 m; *large filled symbols*) and upper mesopelagic zone (125–250 m; *small open symbols*). In panel *a,* the short horizontal black lines indicate the ratios of the aggregation rate constants in the euphotic zone to those in the upper mesopelagic zone (Agg$_{EZ}$:Agg$_{meso}$). In panel *b*, the solid and dashed lines indicate the ordinary least squares fits for the euphotic zone and upper mesopelagic zone, respectively. Aggregation rate constant data are from Dunne et al. (1997); integrated primary production data are from Barber et al. (1996).

Particle dynamics rate constants were estimated during periods characterized by changes in biological productivity in the upper mesopelagic zone from two data sets: the initiation of a spring bloom in the North Atlantic over the course of a month (JGOFS NABE) (Cochran et al. 1993, Murnane et al. 1996) and the seasonal rise and fall of primary productivity in the Ross Sea from spring to autumn over the course of six months (Cochran et al. 2000). Least squares estimates of particle dynamics rate constants during the NABE study (Murnane et al. 1996) had significantly smaller uncertainties compared with the propagated errors from the direct method (Cochran et al. 1993), but both studies found that aggregation and disaggregation rate constants increased over the course of the North Atlantic spring bloom (**Table 3**). This trend is more apparent when the rate constants are plotted as a function of surface nitrate concentrations (**Figure 4**) rather than primary productivity (not shown). The aggregation rate constants increased more quickly than the disaggregation rate constants, such that the β_{-2}/β_2 ratio decreased by a factor of 10 as surface chlorophyll, integrated primary production, and vertical POC flux at 300 m increased and surface nutrients decreased over the course of the bloom.

<COMP: PLEASE INSERT TABLE 3 HERE>

<COMP: PLEASE INSERT FIGURE 4 HERE>

Figure 4 Variations in aggregation rate constants (*red squares*) and ratios of disaggregation to aggregation rate constants (*blue diamonds*) with surface nitrate

concentration from (*a*) the Joint Global Ocean Flux Study (JGOFS) North Atlantic Bloom Experiment (NABE) (Murnane et al. 1996) and (*b*) the JGOFS Ross Sea study (Cochran et al. 2000). Surface nitrate data are from Buesseler et al. (1992a) and Smith et al. (2000) and are plotted in reverse to emphasize the seasonal progression of nutrient drawdown and restoration. Rate estimates and error bars in panel *a* are least squares estimates, and those in panel *b* are the depth-averaged (median) values and 1 standard deviation of the rate constants estimated for each season.**

The Ross Sea was sampled at three different times: (*a*) early in austral spring, when surface nutrients (31 μM NO_3) and primary productivity (74 mmol C/m^2/d) were highest; (*b*) in midsummer, when nutrients had been drawn down significantly (12 μM NO_3) and primary productivity was still high (48–62 mmol C/m^2/d); and (*c*) in autumn, after the growing season had ended, when primary productivity was extremely low (1 mmol C/m^2/d) and nutrients had almost returned to pre-growth-season values (27 μM NO_3) (Cochran et al. 2000, Smith et al. 2000) (**Table 3**). Aggregation and disaggregation rate constants were estimated directly by solving Equation 3 using measurements of ^{234}Th and ^{228}Th for the euphotic and upper mesopelagic zones and assuming a particle sinking speed of 150 m/d. Propagated errors for aggregation rate constants were 1–2 orders of magnitude greater than the estimates themselves and quite variable with depth, so no temporal trends can be deduced with confidence. Errors and variability were lower for estimates of disaggregation rate constants, and there may be a trend toward lower disaggregation rate constants and β_{-2}/β_2 ratios as nutrients are drawn down (**Figure 4**, **Table 3**).

The stronger relationship between β_{-2}/β_2 and surface nutrient drawdown (compared with that between β_{-2}/β_2 and primary productivity) in both the NABE and Ross Sea seasonal data sets may reflect the development of the biogeochemical system that is captured by dissolved nutrients but not by the snapshot of photosynthetic fixation of DIC. This relationship is based on very few and uncertain data, however, so how robust it is in other seasonal systems remains to be seen.

Overall, the thorium-based particle dynamics rate constants suggest that the β_{-2}/β_2 ratio increases with depth and decreases across a spatial gradient in surface biological productivity and over the course of seasonal nutrient drawdown. All else

being equal, a decrease in disaggregation relative to aggregation is expected to promote greater vertical particle flux.

4.4. Other Geochemical Evidence for Particle Dynamics

Although the errors in the dynamical parameter estimates from thorium data are large, they imply continual exchange between the suspended and sinking particle pools throughout the water column, even below the euphotic zone, where particle concentrations quickly decrease and heterotrophic activity that may mediate particle dynamics processes is reduced (see Giering et al. 2014, Steinberg et al. 2008). Given that particle flux and concentrations decrease with depth, it is not surprising that particle destruction processes such as disaggregation occur throughout the water column. It may be more surprising that aggregation processes also occur throughout the water column, even in the abyss, where particle concentrations (and therefore encounter frequencies) are low. However, several lines of evidence from other geochemical tracers suggest that aggregation still occurs in the meso- and bathypelagic zones, as discussed below.

Observations of increasing vertical particle flux with depth, especially of lithogenic components, have been attributed to subsurface lateral transport (Honjo 1982, Honjo et al. 2010, Huang & Conte 2009, Lamborg et al. 2008). Lateral transport has also been invoked to explain old radiocarbon ages of sinking POC (Hwang et al. 2004, 2008). Because the long-distance transport of margin-derived material is likely to be dominated by fine, suspended material, the increasing flux with depth seems to imply deep aggregation processes that allow the incorporation of margin-derived fine, suspended particles into sinking particles.

A study of seasonal POC cycling in the northeast Pacific showed that the $\Delta^{14}C$ content of sinking particles in deep sediment traps decreased at times of higher particle flux (Druffel et al. 1996). This is the opposite of what one might expect, because a higher flux suggests a greater proportion of surface-derived material that is enriched in $\Delta^{14}C$ arriving in the deep sea. The authors attributed this observation to more sorption of $\Delta^{14}C$-depleted DOC to suspended particles and subsequent rapid

exchange between the suspended and sinking particle size fractions during times of high particle flux.

By contrast, a study comparing the amino acid and pigment compositions of suspended and sinking particles during two seasons in the Mediterranean Sea concluded that there was less particle exchange during times of high vertical particle flux in spring (Abramson et al. 2010). Very different compositions, and thus little exchange between size fractions, were observed during the high-flux spring season, when fecal pellets were an important component of sinking particles. The authors suggested that flux periods dominated by fecal pellets, many of which are enclosed in a protective membrane, are less susceptible to disaggregation than phytoplankton aggregates and thus exhibited less particle exchange between the two size fractions. More similar compositions between suspended and sinking particles, indicating more extensive exchange, were observed in the low-flux summer data set.

One way to reconcile the radiocarbon- and biomarker–based conclusions about particle exchange is suggested by another observation based on the organic geochemistry of suspended and sinking particles: Labile compounds, including lipids, amino acids, and undegraded pigments, have been observed in the suspended size fraction in many environments, even at depths greater than 1,000 m (Abramson et al. 2010, Sheridan et al. 2002, Wakeham & Canuel 1988). These labile compounds have estimated decay timescales that are much shorter than the time it would take a suspended particle to sink to the depths at which they are found, suggesting the rapid delivery of fresh material in large marine snow aggregates that disaggregate into the suspended particle pool. Most notably, these studies have suggested that the large-particle class may comprise two functional types of sinking particles: fecal pellets that sink quickly and do not interact with the suspended particle pool, and looser aggregates of fresh algal material that participate more actively in exchange with the suspended particle pool. Both fecal pellets and marine snow aggregates can contribute to periods of high particle flux (Ebersbach & Trull 2008, Ebersbach et al. 2011). The relative proportion of the two sinking particle types at different locations may determine the degree of particle exchange between

the sinking and suspended particle pools and perhaps the efficiency of the biological pump.

Despite the different methodologies used to estimate aggregation and disaggregation rate constants from thorium isotope studies (**Tables 1–3**), the wide range of estimates may nonetheless be consistent with the seasonal radiocarbon and organic biomarker measurements that indicate times of vigorous exchange between the two particle size classes and other times of little exchange.

5. FUTURE DIRECTIONS

The international GEOTRACES program (Anderson et al. 2014) is rapidly increasing the thorium isotope and particle data sets that can be used to estimate particle dynamics parameters (e.g., Hayes et al. 2014, Lam et al. 2014, Owens et al. 2014). These data will allow a more comprehensive assessment of the depth-dependent particle dynamics rate constants as well as their variations across spatial gradients in surface biological productivity, particularly if done consistently with, say, least squares approaches. Moreover, the increased vertical data resolution and the expected analytical errors should reduce the errors in model parameters compared with those of previous studies (Marchal & Lam 2012).

The basic two-size-class model has been criticized for being too simplistic (see Burd 2013, Burd & Jackson 2009), but it has the advantage of being constrained by data. Indeed, simple models may be most appropriate given the paucity of available field data on particle distributions and chemical compositions. To date, biogenic (POC, particulate organic nitrogen) and total particulate mass observations have been quantitatively combined with thorium isotope observations to provide additional constraints on solving for particle dynamics rate constants (e.g., Murnane et al. 1996). The wealth of geochemical measurements from the GEOTRACES program offers the potential to incorporate many more observational constraints. The incorporation of additional constraints may reveal a strategy for increasing the complexity of the basic model to account for missing mechanisms that may not be important for describing thorium but are necessary to explain the behavior of other geochemical tracers. As an example, some of the early conceptual models included

remineralization of large particles (Clegg & Whitfield 1990, Clegg et al. 1991). This additional remineralization term can be justified given zooplankton-mediated aggregation because some of the ingested POC is known to be assimilated and/or respired to CO_2 (Steinberg et al. 2008). A combined treatment of lithogenic particle profiles (see Section 3.4) with POC and thorium may help to separate the loss of large particles caused by disaggregation compared with that caused by remineralization, because titanium present in large particles should not be subject to remineralization.

A further possible extension to the basic two-size-class model would be to test second-order formulations that are more appropriate for physical aggregation mechanisms. Building on this, organic biomarker studies have suggested that the sinking particle size class may itself be separated into two subclasses that have different particle dynamics and thus flux characteristics: (*a*) loose aggregates of marine snow formed from physical aggregation that have high aggregation and disaggregation rates between the small and large particle size classes, and (*b*) tightly packed fecal pellets formed from zooplankton-mediated aggregation that have low exchange between the two particles size classes (Abramson et al. 2010, Wakeham & Canuel 1988). Examinations of sinking particles in polyacrylamide gel traps have shown that these subclasses can be visually distinguished (e.g., Ebersbach & Trull 2008, Ebersbach et al. 2011).

Assessing the importance of each particle class as a function of pelagic ecosystem structure (e.g., Michaels & Silver 1988) may be a key to understanding the interplay between particle dynamics and the strength and efficiency of the biological pump. It is not clear whether the data exist to adequately constrain a model with one suspended and two sinking particle classes. However, such a model would be a step toward synthesizing the insights gained from the three approaches for studying particle dynamics described in Section 2. Separating sinking particles into those that are formed physically and those that are formed biologically would help in matching up the data-based inverse estimates of bulk dynamical parameters with the forward, mechanistically based measurements and estimates of physical and biological processes from the first two approaches described in Section 2. Moreover, guidance

may then be provided on the appropriate mechanisms to consider and the appropriate measurements to make in order to better understand the biological pump.

SUMMARY POINTS

1. Multiple geochemical tracers (e.g., thorium isotopes, radiocarbon, and organic biomarkers) support the idea of two functional particle classes: small, suspended particles with long residence times (which constitute most of the particle mass) and large, sinking particles with short turnover times (which contribute most of the particle flux).

2. A simple particle dynamics framework in which small particles are suspended and interact with the dissolved phase, large particles are removed by sinking, and small and large particles interact via aggregation and disaggregation seems to be sufficient for understanding the vertical profiles of thorium isotopes, particulate organic carbon, particulate barium, and lithogenic particles in the ocean. Differences in profile shapes between the various components seem to arise from different sources and from varying interactions between the dissolved and suspended particle phases.

3. Quantitative constraints on particle dynamics have come from the combination of simple models with measurements of dissolved and particulate thorium isotopes, whose well-defined sources help to produce estimates of net particle aggregation and disaggregation. The paucity of data has so far resulted in estimates of dynamical parameters with very large errors, but new measurements from the ongoing GEOTRACES program has the potential to improve the estimates and reduce the errors significantly.

4. Although estimated rate constants span a large range, some trends are apparent: Aggregation and disaggregation rate constants tend to decrease with depth, leading to turnover times of suspended particles with respect to aggregation of days to weeks in the euphotic zone and months to years in the meso- and bathypelagic zones. Large particles have extremely short turnover times of hours

to days. Finally, the ratio of disaggregation to aggregation tends to increase with depth and decrease with increasing integrated primary production.

5. Other geochemical tracers, including lithogenic elements and organic biomarkers, suggest ways to increase the complexity of the basic particle dynamics framework.

LITERATURE CITED

Abramson L, Lee C, Liu ZF, Wakeham SG, Szlosek J. 2010. Exchange between suspended and sinking particles in the northwest Mediterranean as inferred from the organic composition of in situ pump and sediment trap samples. *Limnol. Oceanogr.* 55:725–39

Alldredge AL, Gotschalk C. 1988. In situ settling behavior of marine snow. *Limnol. Oceanogr.* 33:339–51

Anderson RF. 2003. Chemical tracers of particle transport. In *Treatise on Geochemistry*, Vol. 6: *The Oceans and Marine Geochemistry,* ed. H Elderfield, pp. 247–73. Amsterdam: Elsevier

Anderson RF, Mawji E, Cutter GA, Measures CI, Jeandel C. 2014. GEOTRACES: Changing the way we explore ocean chemistry. *Oceanography* 27(1):50–61

Athias V, Mazzega P, Jeandel C. 2000a. Nonlinear inversions of a model of the oceanic dissolved-particulate exchanges. In *Inverse Methods in Global Biogeochemical*

Cycles, ed. P Kasibhatla, M Heimann, P Rayner, N Mahowald, RG Prinn, DE Hartley, pp. 205–22. Washington, DC: Am. Geophys. Union

Athias V, Mazzega P, Jeandel C. 2000b. Selecting a global optimization method to estimate the oceanic particle cycling rate constants. *J. Mar. Res.* 58:675–707

Bacon MP, Anderson RF. 1982. Distribution of thorium isotopes between dissolved and particulate forms in the deep sea. *J. Geophys. Res.* 87:2045–56

Bacon MP, Huh C-A, Fleer AP, Deuser WG. 1985. Seasonality in the flux of natural radionuclides and plutonium in the deep Sargasso Sea. *Deep-Sea Res. A* 32:273–86

Barber RT, Sanderson MP, Lindley ST, Chai F, Newton J, et al. 1996. Primary productivity and its regulation in the equatorial Pacific during and following the 1991–1992 El Nino. *Deep-Sea Res. II* 43:933–69

Bishop JKB. 1988. The barite-opal-organic carbon association in oceanic particulate matter. *Nature* 332:341–43

Bishop JKB, Edmond JM, Ketten DR, Bacon MP, Silker WB. 1977. Chemistry, biology, and vertical flux of particulate matter from upper 400 m of equatorial Atlantic Ocean. *Deep-Sea Res.* 24:511–48

Bishop JKB, Lam PJ, Wood TJ. 2012. Getting good particles: accurate sampling of particles by large volume in-situ filtration. *Limnol. Oceanogr. Methods* 10:681–710

Bishop JKB, Wood TJ. 2008. Particulate matter chemistry and dynamics in the twilight zone at VERTIGO ALOHA and K2 sites. *Deep-Sea Res. I* 55:1684–706

Boyd PW, Trull TW. 2007. Understanding the export of biogenic particles in oceanic waters: Is there consensus? *Prog. Oceanogr.* 72:276–312

Brun-Cottan JC. 1986. Vertical transport of particles within the ocean. In *The Role of Air-Sea Exchange in Geochemical Cycling*, ed. P Buat-Ménard, pp. 83–111. Dordrecht, Neth.: Reidel

Buck CS, Landing WM, Resing JA. 2010. Particle size and aerosol iron solubility: a high-resolution analysis of Atlantic aerosols. *Mar. Chem.* 120:14–24

Buesseler KO, Andrews JA, Hartman MC, Belastock R, Chai F. 1995. Regional estimates of the export flux of particulate organic carbon derived from thorium-234 during the JGOFS EqPac program. *Deep-Sea Res. II* 42:777–91

Buesseler KO, Antia AN, Chen M, Fowler SW, Gardner WD, et al. 2007. An assessment of the use of sediment traps for estimating upper ocean particle fluxes. *J. Mar. Res.* 65:345–416

Buesseler KO, Bacon MP, Cochran JK, Livingston HD. 1992a. Carbon and nitrogen export during the JGOFS North Atlantic Bloom experiment estimated from [234]Th:[238]U disequilibria. *Deep-Sea Res. A* 39:1115–37

Buesseler KO, Boyd PW. 2009. Shedding light on processes that control particle export and flux attenuation in the twilight zone of the open ocean. *Limnol. Oceanogr.* 54:1210–32

Buesseler KO, Cochran JK, Bacon MP, Livingston HD, Casso SA, et al. 1992b. Determination of thorium isotopes in seawater by nondestructive and radiochemical procedures. *Deep-Sea Res. A* 39:1103–14

Burd AB. 2013. Modeling particle aggregation using size class and size spectrum approaches. *J. Geophys. Res.* 118:3431–43

Burd AB, Jackson GA. 2009. Particle aggregation. *Annu. Rev. Mar. Sci.* 1:65–90

Chipman DW, Marra J, Takahashi T. 1993. Primary production at 47°N and 20°W in the North Atlantic Ocean: a comparison between the ^{14}C incubation method and the mixed layer carbon budget. *Deep-Sea Res. II* 40:151–69

Clegg SL, Bacon MP, Whitfield M. 1991. Application of a generalized scavenging model to thorium isotope and particle data at equatorial and high-latitude sites in the Pacific Ocean. *J. Geophys. Res.* 96:20655–70

Clegg SL, Whitfield M. 1990. A generalized model for the scavenging of trace metals in the open ocean—I. Particle cycling. *Deep-Sea Res. A* 37:809–32

Clegg SL, Whitfield M. 1991. A generalized model for the scavenging of trace metals in the open ocean—II. Thorium scavenging. *Deep-Sea Res. A* 38:91–120

Clegg SL, Whitfield M. 1993. Application of a generalized scavenging model to time series [234]Th and particle data obtained during the JGOFS North Atlantic bloom experiment. *Deep-Sea Res. I* 40:1529–45

Cochran JK, Buesseler KO, Bacon MP, Livingston HD. 1993. Thorium isotopes as indicators of particle dynamics in the upper ocean: results from the JGOFS North-Atlantic Bloom Experiment. *Deep-Sea Res. I* 40:1569–95

Cochran JK, Buesseler KO, Bacon MP, Wang HW, Hirschberg DJ, et al. 2000. Short-lived thorium isotopes (^{234}Th, ^{228}Th) as indicators of POC export and particle cycling in the Ross Sea, Southern Ocean. *Deep-Sea Res. II* 47:3451–90

Cochran JK, Livingston HD, Hirschberg DJ, Surprenant LD. 1987. Natural and anthropogenic radionuclide distributions in the northwest Atlantic Ocean. *Earth Planet. Sci. Lett.* 84:135–52

Cutter GA. 2013. Intercalibration in chemical oceanography—getting the right number. *Limnol. Oceanogr. Methods* 11:418–24

Dammshäuser A, Wagener T, Garbe-Schönberg D, Croot P. 2013. Particulate and dissolved aluminum and titanium in the upper water column of the Atlantic Ocean. *Deep-Sea Res. I* 73:127–39

Dehairs F, Chesselet R, Jedwab J. 1980. Discrete suspended particles of barite and the barium cycle in the open ocean. *Earth Planet. Sci. Lett.* 49:528–50

Dehairs F, Jacquet S, Savoye N, Van Mooy BAS, Buesseler KO, et al. 2008. Barium in twilight zone suspended matter as a potential proxy for particulate organic carbon remineralization: results for the North Pacific. *Deep-Sea Res. II* 55:1673–83

Druffel ERM, Bauer JE, Williams PM, Griffin S, Wolgast D. 1996. Seasonal variability of particulate organic radiocarbon in the northeast Pacific ocean. *J. Geophys. Res.* 101:20543–52

Druffel ERM, Williams PM. 1990. Identification of a deep marine source of particulate organic carbon using bomb ^{14}C. *Nature* 347:172–74

Dunne JP, Murray JW, Young J, Balistrieri LS, Bishop J. 1997. ^{234}Th and particle cycling in the central equatorial Pacific. *Deep-Sea Res. II* 44:2049–83

Dymond J, Suess E, Lyle M. 1992. Barium in deep-sea sediment: a geochemical proxy for paleoproductivity. *Paleoceanography* 7:163–81

Ebersbach F, Trull T. 2008. Sinking particle properties from polyacrylamide gels during the KErguelen Ocean and Plateau compared Study (KEOPS): zooplankton control of carbon export in an area of persistent natural iron inputs in the Southern Ocean. *Limnol. Oceanogr.* 53:212–24

Ebersbach F, Trull TW, Davies DM, Bray SG. 2011. Controls on mesopelagic particle fluxes in the Sub-Antarctic and Polar Frontal Zones in the Southern Ocean south of

Australia in summer—perspectives from free-drifting sediment traps. *Deep-Sea Res. II* 58:2260–76

Engel A, Szlosek J, Abramson L, Liu Z, Lee C. 2009. Investigating the effect of ballasting by $CaCO_3$ in *Emiliania huxleyi*: I. Formation, settling velocities and physical properties of aggregates. *Deep-Sea Res. II* 56:1396–407

Eppley RW, Renger EH, Betzer PR. 1983. The residence time of particulate organic carbon in the surface layer of the ocean. *Deep-Sea Res. A* 30:311–23

Fowler SW, Knauer GA. 1986. Role of large particles in the transport of elements and organic compounds through the oceanic water column. *Prog. Oceanogr.* 16:147–94

François R, Honjo S, Krishfield R, Manganini S. 2002. Factors controlling the flux of organic carbon to the bathypelagic zone of the ocean. *Glob. Biogeochem. Cycles* 16:1087

François R, Honjo S, Manganini SJ, Ravizza GE. 1995. Biogenic barium fluxes to the deep sea: implications for paleoproductivity reconstruction. *Glob. Biogeochem. Cycles* 9:289–303

Giering SLC, Sanders R, Lampitt RS, Anderson TR, Tamburini C, et al. 2014. Reconciliation of the carbon budget in the ocean's twilight zone. *Nature* 507:480–83

Hayes CT, Anderson RF, Fleisher MQ, Huang K-F, Robinson LF, et al. 2014. [230]Th and [231]Pa on GEOTRACES GA03, the U.S. GEOTRACES North Atlantic Transect, and implications for modern and paleoceanographic chemical fluxes. *Deep-Sea Res. II*. In press

Honjo S. 1982. Seasonality and interaction of biogenic and lithogenic particulate flux at the Panama Basin. *Science* 218:883–84

Honjo S, Krishfield RA, Eglinton TI, Manganini SJ, Kemp JN, et al. 2010. Biological pump processes in the cryopelagic and hemipelagic Arctic Ocean: Canada Basin and Chukchi Rise. *Prog. Oceanogr.* 85:137–70

Honjo S, Manganini SJ. 1993. Annual biogenic particle fluxes to the interior of the North Atlantic Ocean; studied at 34°N 21°W and 48°N 21°W. *Deep-Sea Res. II* 40:587–607

Huang S, Conte MH. 2009. Source/process apportionment of major and trace elements in sinking particles in the Sargasso Sea. *Geochim. Cosmochim. Acta* 73:65–90

Hwang J, Druffel ERM, Griffin S, Smith KL, Baldwin RJ, Bauer JE. 2004. Temporal
variability of $\Delta^{14}C$, $\delta^{13}C$, and C/N in sinking particulate organic matter at a deep time
series station in the northeast Pacific Ocean. *Glob. Biogeochem. Cycles* 18:GB4015

Hwang J, Eglinton TI, Krishfield RA, Manganini SJ, Honjo S. 2008. Lateral organic
carbon supply to the deep Canada Basin. *Geophys. Res. Lett.* 35: L11607

Iversen MH, Ploug H. 2010. Ballast minerals and the sinking carbon flux in the ocean:
carbon-specific respiration rates and sinking velocity of marine snow aggregates.
Biogeosciences 7:2613–24

Jeandel C, Rutgers van der Loeff M, Lam PJ, Roy-Barman M, Sherrell RM, et al. 2014.
What did we learn on the oceanic particle dynamic from the GEOSECS-JGOFS
times? *Prog. Oceanogr.* In review

Jeandel C, Tachikawa K, Bory A, Dehairs F. 2000. Biogenic barium in suspended and
trapped material as a tracer of export production in the tropical NE Atlantic
(EUMELI sites). *Mar. Chem.* 71:125–42

Komar PD, Morse AP, Small LF, Fowler SW. 1981. An analysis of sinking rates of
natural copepod and euphausiid fecal pellets. *Limnol. Oceanogr.* 26:172–80

Kwon EY, Primeau F, Sarmiento JL. 2009. The impact of remineralization depth on the
air-sea carbon balance. *Nat. Geosci.* 2:630–35

Lam PJ, Bishop JKB. 2007. High biomass, low export regimes in the Southern Ocean.
Deep-Sea Res. II 54:601–38

Lam PJ, Doney SC, Bishop JKB. 2011. The dynamic ocean biological pump: insights
from a global compilation of particulate organic carbon, $CaCO_3$, and opal
concentration profiles from the mesopelagic. *Glob. Biogeochem. Cycles* 25:GB3009

Lam PJ, Ohnemus DC, Auro ME. 2014. Size fractionated major particle composition and
mass from the US GEOTRACES North Atlantic Zonal Transect. *Deep-Sea Res. II.* In
review

Lamborg CH, Buesseler KO, Lam PJ. 2008. Sinking fluxes of minor and trace elements
in the North Pacific Ocean measured during the VERTIGO program. *Deep-Sea Res.
II* 55:1564–77

Lavelle JW, Cudaback CN, Paulson AJ, Murray JW. 1991. A rate for the scavenging of
fine particles by macroaggregates in a deep estuary. *J. Geophys. Res.* 96:783–90

Marchal O, Lam PJ. 2012. What can paired measurements of Th isotope activity and particle concentration tell us about particle cycling in the ocean? *Geochim. Cosmochim. Acta* 90:126–48

McCave IN. 1975. Vertical flux of particles in the ocean. *Deep-Sea Res. Oceanogr. Abstr.* 22:491–502

McCave IN. 1984. Size spectra and aggregation of suspended particles in the deep ocean. *Deep-Sea Res. A* 31:329–52

McDonnell AMP, Buesseler KO. 2010. Variability in the average sinking velocities of marine particles. *Limnol. Oceanogr.* 55:2085–96

McDonnell AMP, Lam PJ, Lamborg CH, Buesseler KO, Sanders R, et al. 2014. The oceanographic toolbox for the collection of sinking and suspended marine particles. *Prog. Oceanogr.* In review

Mercier H. 1986. Determining the general circulation of the ocean: a nonlinear inverse problem. *J. Geophys. Res.* 91:5103–9

Michaels AF, Silver MW. 1988. Primary production, sinking fluxes and the microbial food web. *Deep-Sea Res. A* 35:473–90

Murnane RJ. 1994. Determination of thorium and particulate matter cycling parameters at station P: a reanalysis and comparison of least squares techniques. *J. Geophys. Res.* 99:3393–405

Murnane RJ, Cochran JK, Buesseler KO, Bacon MP. 1996. Least-squares estimates of thorium, particle, and nutrient cycling rate constants from the JGOFS North Atlantic Bloom Experiment. *Deep-Sea Res. I* 43:239–58

Murnane RJ, Cochran JK, Sarmiento JL. 1994. Estimates of particle- and thorium-cycling rates in the northwest Atlantic Ocean. *J. Geophys. Res.* 99:3373–92

Murnane RJ, Sarmiento JL, Bacon MP. 1990. Thorium isotopes, particle cycling models, and inverse calculations of model rate constants. *J. Geophys. Res.* 95:16195–206

Murray JW, Downs JN, Strom S, Wei C-L, Jannasch HW. 1989. Nutrient assimilation, export production and [234]Th scavenging in the eastern equatorial Pacific. *Deep-Sea Res. A* 36:1471–89

Murray RW, Leinen M. 1996. Scavenged excess aluminum and its relationship to bulk titanium in biogenic sediment from the central equatorial Pacific Ocean. *Geochim. Cosmochim. Acta* 60:3869–78

Newton J, Van Voorhis K. 2002. *Seasonal patterns and controlling factors of primary production in Puget Sound's Central Basin and Possession Sound.* Publ. 02-03-059, Wash. State Dep. Ecol., Olympia

Nozaki Y, Horibe Y, Tsubota H. 1981. The water column distributions of thorium isotopes in the western North Pacific. *Earth Planet. Sci. Lett.* 54:203–16

Nozaki Y, Yang H-S, Yamada M. 1987. Scavenging of thorium in the ocean. *J. Geophys. Res.* 92:772–78

Ohnemus DC, Lam PJ. 2014. Cycling of lithogenic marine particulates in the US GEOTRACES North Atlantic Zonal Transect. *Deep-Sea Res. II.* In review

Owens SA, Pike S, Buesseler KO. 2014. Thorium-234 as a tracer of particle dynamics and upper ocean export in the Atlantic Ocean. *Deep-Sea Res. II.* In press

Paytan A, Griffith EM. 2007. Marine barite: recorder of variations in ocean export productivity. *Deep-Sea Res. II* 54:687–705

Peterson ML, Wakeham SG, Lee C, Askea MA, Miquel JC. 2005. Novel techniques for collection of sinking particles in the ocean and determining their settling rates. *Limnol. Oceanogr. Methods* 3:520–32

Ratmeyer V, Balzer W, Bergametti G, Chiapello I, Fischer G, Wyputta U. 1999. Seasonal impact of mineral dust on deep-ocean particle flux in the eastern subtropical Atlantic Ocean. *Mar. Geol.* 159:241–52

Sheridan CC, Lee C, Wakeham SG, Bishop JKB. 2002. Suspended particle organic composition and cycling in surface and midwaters of the equatorial Pacific Ocean. *Deep-Sea Res. I* 49:1983–2008

Smith WO, Marra J, Hiscock MR, Barber RT. 2000. The seasonal cycle of phytoplankton biomass and primary productivity in the Ross Sea, Antarctica. *Deep-Sea Res. II* 47:3119–40

Steinberg DK, Van Mooy BAS, Buesseler KO, Boyd PW, Kobari T, Karl DM. 2008. Bacterial vs. zooplankton control of sinking particle flux in the ocean's twilight zone. *Limnol. Oceanogr.* 53:1327–38

Stemmann L, Boss E. 2012. Plankton and particle size and packaging: from determining optical properties to driving the biological pump. *Annu. Rev. Mar. Sci.* 4:263–90

Tarantola A, Valette B. 1982. Generalized nonlinear inverse problems solved using the least squares criterion. *Rev. Geophys.* 20:219–32

Volk T, Hoffert MI. 1985. Ocean carbon pumps: Analysis of relative strengths and efficiencies in ocean-driven atmospheric CO_2 changes. *Geophysical Monographs* 32: 99-110

Wakeham SG, Canuel EA. 1988. Organic geochemistry of particulate matter in the eastern tropical North Pacific Ocean: implications for particle dynamics. *J. Mar. Res.* 46:183–213

Westberry T, Behrenfeld MJ, Siegel DA, Boss E. 2008. Carbon-based primary productivity modeling with vertically resolved photoacclimation. *Glob. Biogeochem. Cycles* 22:GB2024

Wunsch C. 2006. *Discrete Inverse and State Estimation Problems: With Geophysical Fluid Applications*. Cambridge, UK: Cambridge Univ. Press

Table 1 Summary of thorium data sets in which particle aggregation and disaggregation rate constants have been estimated

Data set	Data collection period	Isotope	Data reference	Type of environment	Rate estimate reference	Rate estimate method	Depth range (m)	Agg. (per year)	Disagg. (per year)	Disagg. :agg.	Sinking (m/d)[a]	Note[b]	Inte prii pro (mn C/m²
Northwest Pacific	September 1984	^{230}Th	Nozaki et al. 1987	Western subarctic Pacific	Nozaki et al. 1987	Direct	1,100–5,500	2.5–12.3	148–788	60–64	100	G	38–
Nares Abyssal Plain	September 1984	^{228}Th, ^{230}Th	Cochran et al. 1987	Oligotrophic northwest Atlantic	Murnane et al. 1994	Least squares (total inversion)	25–5,500	8–18	580–2,690	36–299	165	D	17
Puget Sound	July 1984, April 1985	^{234}Th	Lavelle et al. 1991	Coastal inlet	Lavelle et al. 1991	Direct	10–200	63–85	158–568	3–7	100	S	62
Eastern equatorial Pacific	June 1987	^{234}Th	Murray et al. 1989	Upwelling (stations 1 and 2), oligotrophic (station 5)	Clegg et al. 1991	Direct	20–450	0.02–49	16–4,996	2–3,729	100	G, D	28–
Ocean Station Papa	October 1987	^{234}Th, ^{230}Th,	M.P. Bacon, unpublished data	Eastern subarctic Pacific	Murnane et al. 1990	Least squares (Wolberg)	1,000–3,800	0.2	0.8	4	100	NA	38

		[228]Th			Murnane 1994	Least squares (total inversion)	1,000–3,800	0.8	400	500	100	NA	38
					Clegg et al. 1991	Direct	25–3,800	0.5–52	64–640[d]	22–90	100	D	38
JGOFS NABE	April–May 1989	[234]Th	Buesseler et al. 1992a	North Atlantic spring bloom	Cochran et al. 1993	Direct	150–300	1.1–33.2	126–407	12–115	150	S	87–
		[228]Th	Buesseler et al. 1992b	North Atlantic spring bloom	Cochran et al. 1993	Direct	150–300	−0.5–19.7	108–281	−212–14	150	S	87–
		[234]Th, [228]Th, [230]Th	Buesseler et al. 1992a,b	North Atlantic spring bloom	Murnane et al. 1996	Least squares (total inversion)	150–300	2–76	156–524	7–78	150	S	87–
JGOFS EqPac	August–September 1992	[234]Th	Murray & Leinen 1996	Central equatorial Pacific	Dunne et al. 1997	Direct	125–250	265–603	1,825[e]	3–7	NA	G	24–1
JGOFS Ross Sea	November 1996–February 1997	[234]Th, [228]Th	Cochran et al. 2000	Antarctic marginal sea	Cochran et al. 2000	Direct	5–205	15–354	142–5,037	0.4–163	150	D, S	1–7

Abbreviations: agg., aggregation rate constant; disagg., disaggregation rate constant; EqPac, Equatorial Pacific Process Study; integr. prim. prod., integrated primary production; JGOFS, Joint Global Ocean Flux Study; NA, not applicable; NABE, North Atlantic Bloom Experiment.

[a]All sinking rates were assumed except in the Nares Abyssal Plain data set.

[b]Source of range in rate constants: G, geographical variation (multiple stations); D, depth variation; S, seasonal progression.

[c]Values for the northwest Pacific, Puget Sound, and Ocean Station Papa were estimated from monthly net primary production using the updated carbon-based productivity model of Westberry et al. (2008). Values for the other data sets were measured on their respective cruises: Nares Abyssal Plain, Newton & Van Voorhis (2002); eastern equatorial Pacific, Murray et al. (1989); JGOFS NABE, Chipman et al. (1993); JGOFS EqPac, Barber et al. (1996); JGOFS Ross Sea, Smith et al. (2000).

[d]Disaggregation rate constants are from the average eastern equatorial Pacific values (Clegg et al. 1991).

[e]Assumed disaggregation rate constant.

Table 2 Depth trends in particle dynamics rate constants and turnover times

Depth range (m)	Agg. (per year)	Disagg. (per year)	Disagg.:Agg.	τ_{agg} (days)	τ_{disagg} (days)
Eastern equatorial Pacific station 1					
25–80	8.4 ± 24	664 ± 1652	79 ± 303	44	0.6
80–200	0.12 ± 0.1	123 ± 14	991 ± 1085	2,951	3
200–450	0.04 ± 0.03	60 ± 5	$1,588 \pm 1240$	9,628	6
Eastern equatorial Pacific station 5					
25–80	39	$2,809 \pm 3,093$	72	9	0.13
80–200	2.6 ± 0.7	292 ± 37	114 ± 35	143	1.3
200–450	0.24 ± 0.005	66 ± 12	278 ± 50	1542	5.6
Ocean Station Papa					
35–80	30 ± 15	$664 \pm 1,839$	22 ± 57	12	0.5
80–200	10 ± 4	260 ± 487	27 ± 10	38	1.4
200–1,000	1.6 ± 0.5	64 ± 10	39 ± 13	223	5.7
1,000–4,000	0.7 ± 0.08	64 ± 10	90 ± 12	514	5.7
Nares Abyssal Plain					
0–200	11 ± 2	$2,283 \pm 405$	217 ± 55	33.2	0.2
200–800	17 ± 1	800 ± 195	47 ± 12	21.5	0.5
800–5,500	9 ± 1	836 ± 111	91 ± 15	39.3	0.4

Data for the two eastern equatorial Pacific stations and Ocean Station Papa are from Clegg et al. (1991); data for the Nares Abyssal Plain are from Murnane et al. (1994). Data are grouped in similar depth ranges to facilitate comparison. The reported rate constants are median ± 1 standard deviation of values in the depth range. To calculate the aggregation rate constants at Ocean Station Papa, Clegg et al. (1991) applied median disaggregation rate constants from three eastern equatorial Pacific stations. Abbreviations: agg., aggregation rate constant; disagg., disaggregation rate constant; τ_{agg}, turnover time with respect to aggregation; τ_{disagg}, turnover time with respect to disaggregation.
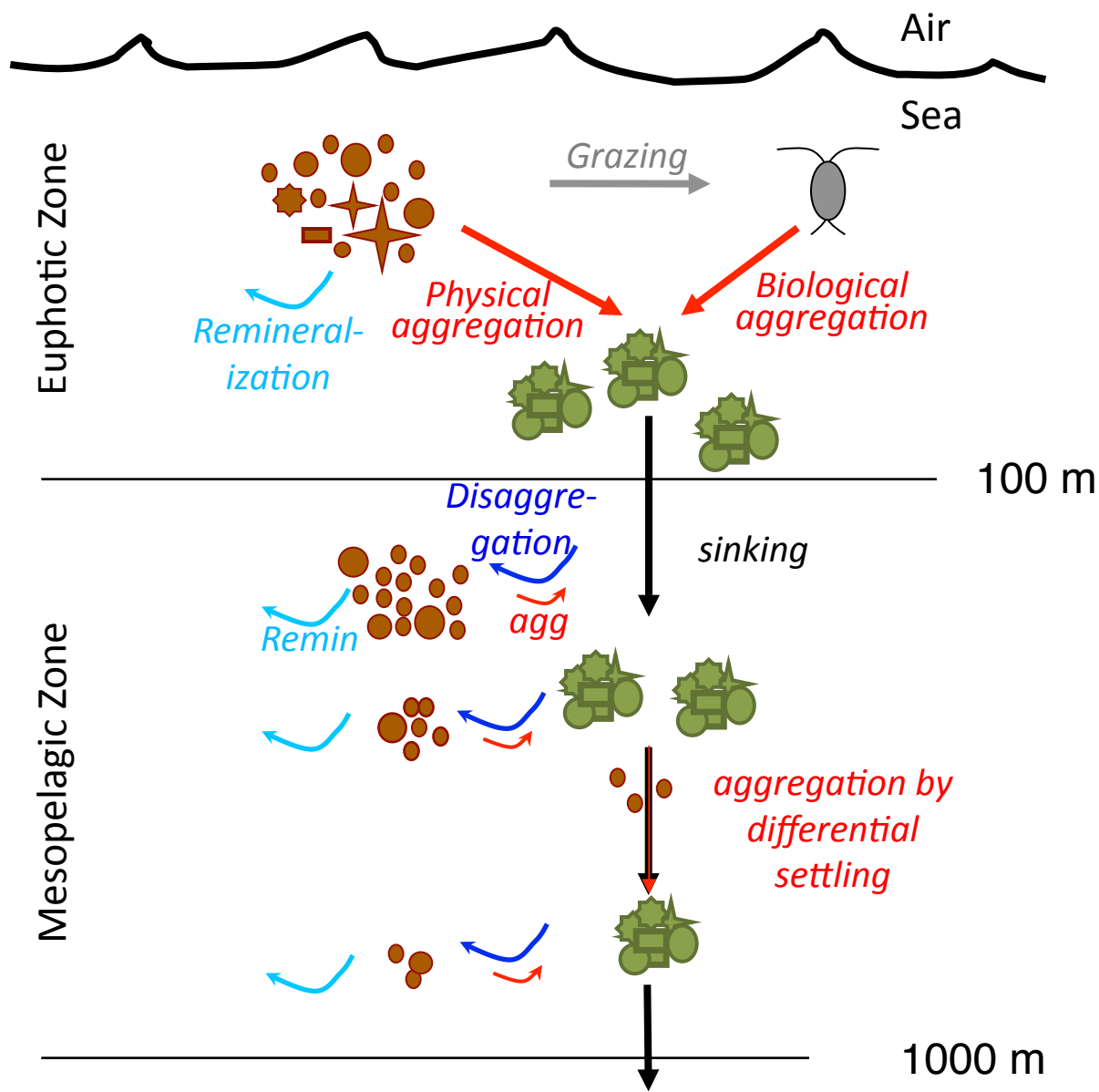
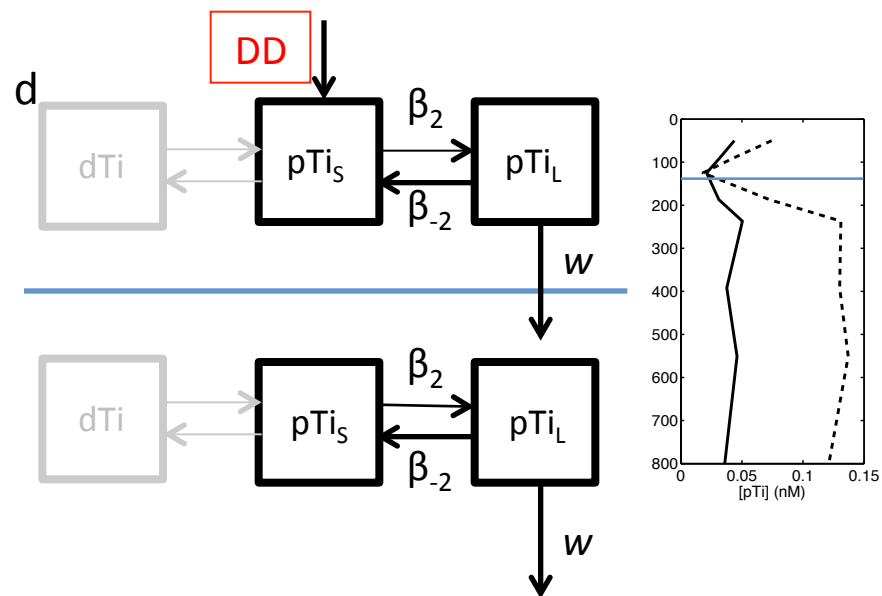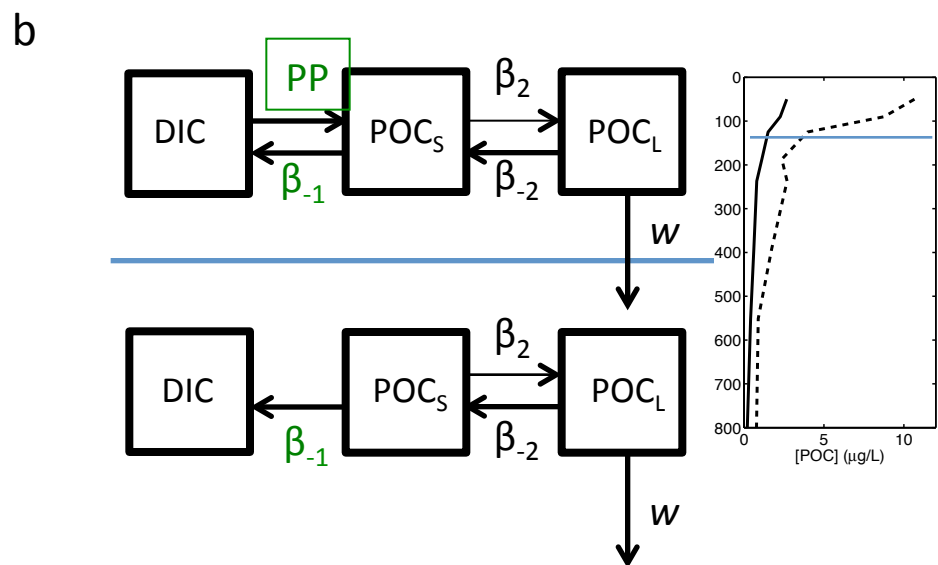Table 3 Seasonal trends in particle dynamics rate constants and turnover times
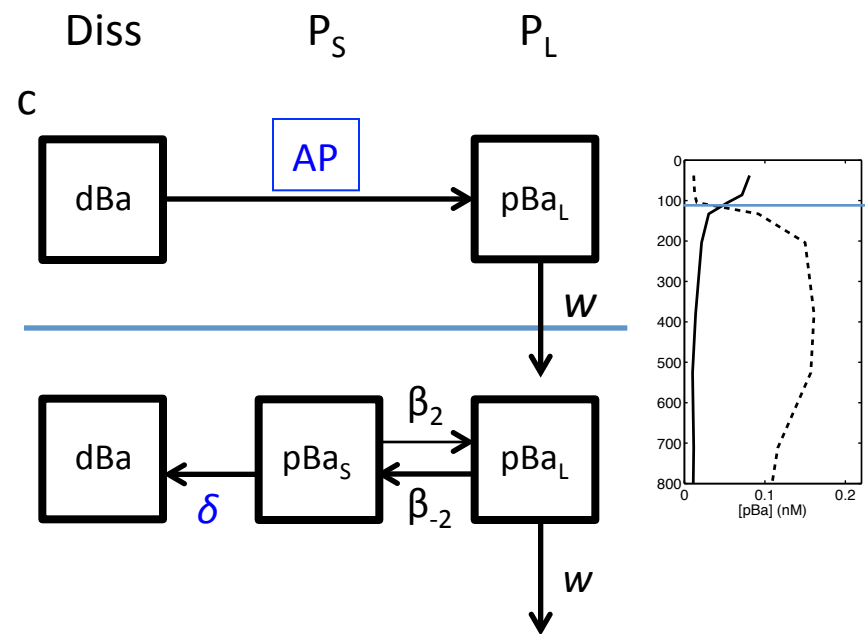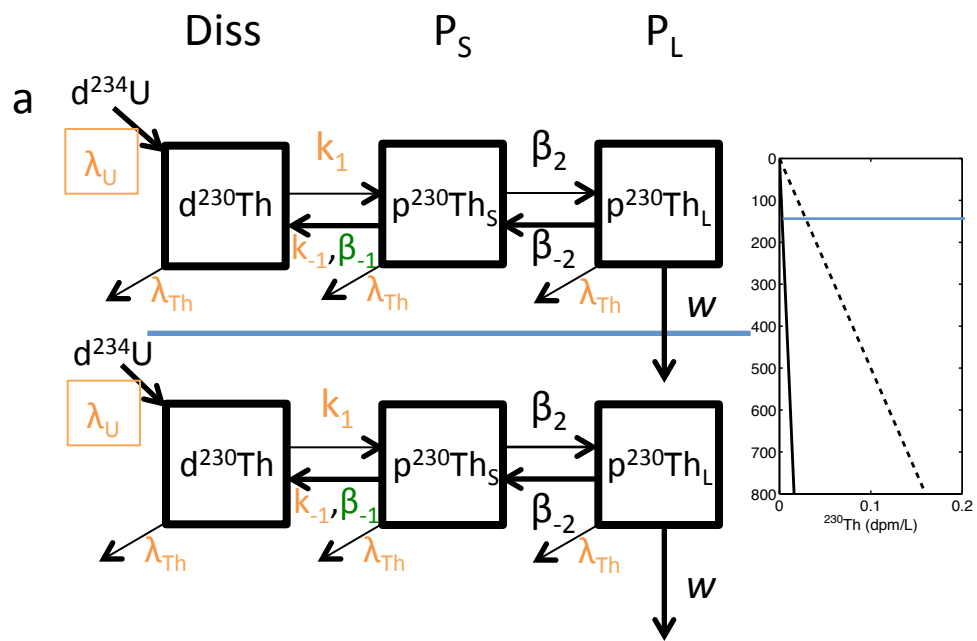
Sampling date	Depth range (m)	[NO$_3$] (μM)[a]	Integr. prim. prod. (mmol C/m^2/d)[a]	Agg. ± 1 SD (per year)	Disagg. ± 1 SD	Disagg.:Agg. ±1 SD	τ_{agg} (days)	τ_{disagg} (days)
JGOFS NABE								
April 24, 1989	150–300	6	91	2 ± 0.2	156 ± 17	87 ± 12	182.5	2.3
May 7, 1989	150–300	4.5	98	12 ± 1	321 ± 32	27 ± 4	30.4	1.1
May 22, 1989	150–300	0.5	87	76 ± 9	524 ± 74	7 ± 1	4.8	0.7
JGOFS Ross Sea								
November 2, 1996	10–305	31	74	175 ± 97	4,088 ± 2,140	22 ± 97	2.1	0.09
January 19 and February 1, 1997	5–205	11 (Jan. 19) 12 (Feb. 1)	62 (Jan. 19) 48 (Feb. 1)	106 ± 154	438 ± 1,358	4 ± 154	3.4	0.83
April 14 and 23, 1997	5–83	27 (Apr. 14) 27 (Apr. 23)	1.5 (Apr. 14) 1 (Apr. 23)	51 ± 147	2373 ± 932	20 ± 147	7.2	0.15

Data for the JGOFS NABE study are primarily from Murnane et al. (1996); data for the JGOFS Ross Sea study are primarily from Cochran et al. (2000). JGOFS NABE rate constants are the least squares solution ± 1 standard deviation. JGOFS Ross Sea rate constants are median values of rate constants estimated analytically in the depth range ± 1 standard deviation of values in the depth range; note that propagated error estimates for each rate were typically much greater than the standard deviations reported here. Abbreviations: agg., aggregation rate constant; disagg. disaggregation rate constant; integr. prim. prod., integrated primary productivity; JGOFS, Joint Global Ocean Flux Study; NABE, North Atlantic Bloom Experiment.
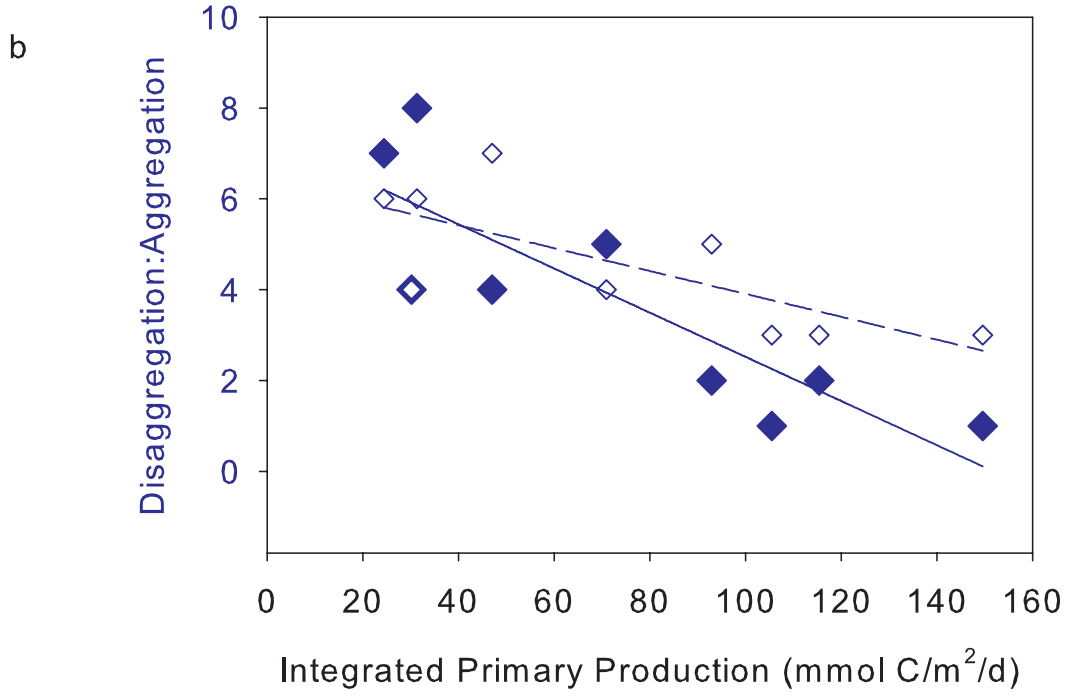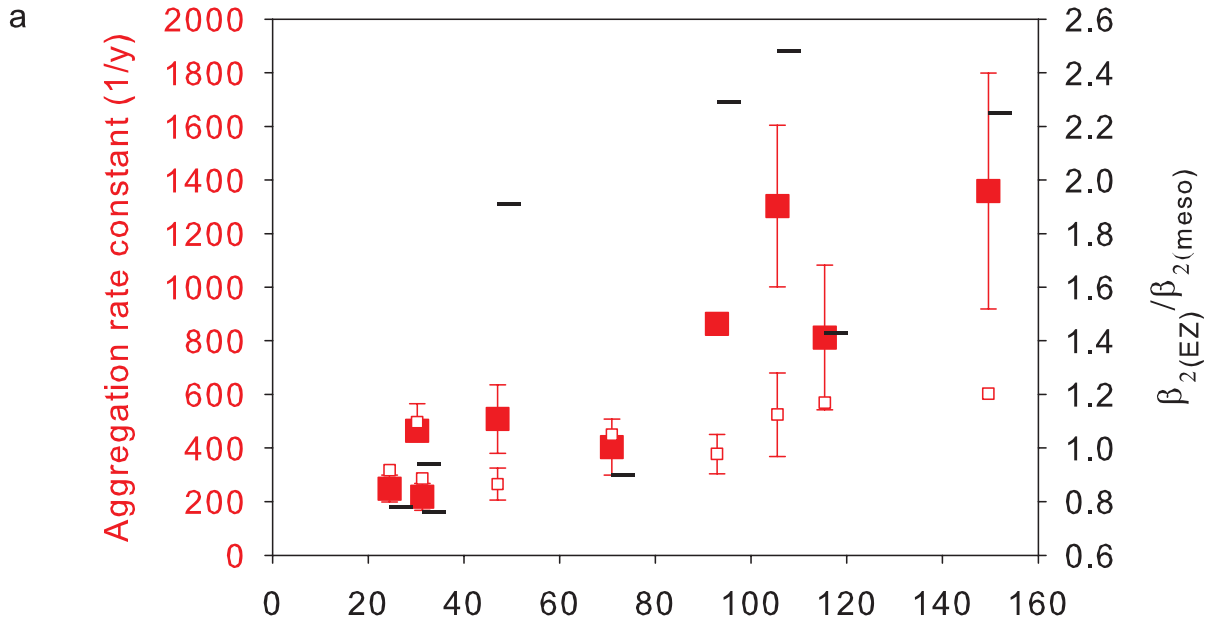
[a]Surface NO$_3$ and integrated primary productivity data are from Buesseler et al. (1992a) for the JGOFS NABE study and from Smith et al. (2000) for the JGOFS Ross Sea study.
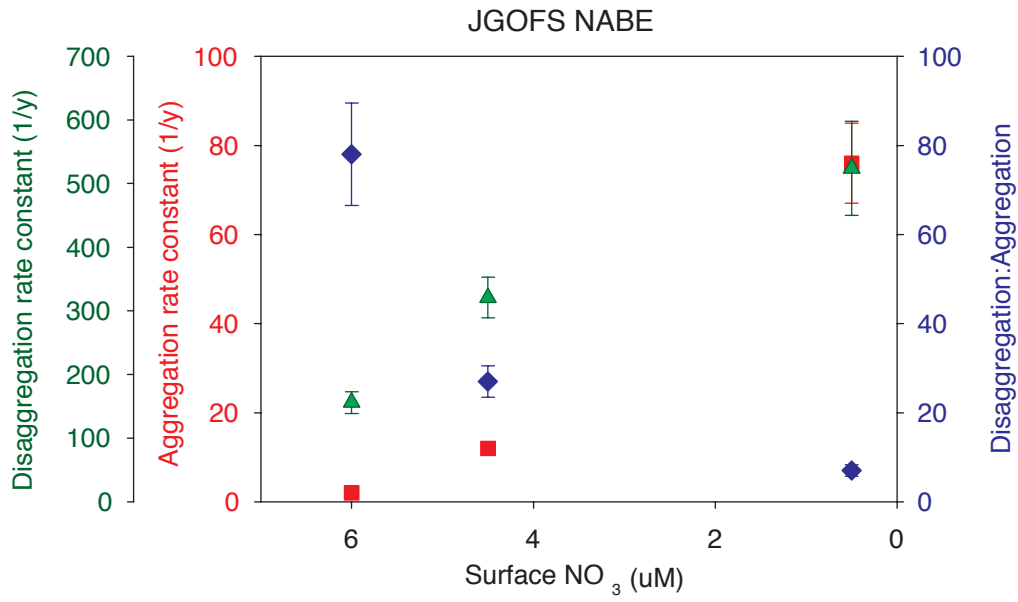
JGOFS EqPac Survey II

a

JGOFS NABE

Disaggregation rate constant (1/y)
Aggregation rate constant (1/y)
Disaggregation:Aggregation

Surface NO$_3$ (uM)

b

JGOFS Ross Sea

Disaggregation rate constant (1/y)
Aggregation rate constant (1/y)
Disaggregation:Aggregation

Surface NO$_3$ (uM)